# Phase Behavior of Homologous Perfluoropolyether Surfactants: NMR, SAXS, and Optical Microscopy

**Stefania Mele,[†] Barry William Ninham,[‡] and Maura Monduzzi*[,†]**

*Department of Chemical Sciences, CSGI-Cagliari University, S.S. 554 Bivio Sestu, 09042 Monserrato, Italy, and Department of Applied Mathematics, Australia National University, Canberra, Australia*

*Received: January 21, 2004; In Final Form: June 18, 2004*

Self-assembled structures formed by perfluoropolyether (PFPE) carboxylates with hydrophobic chain terminated by $Cl-C_3F_6O$, and either sodium or ammonium counterions, have been explored in aqueous binary systems. The focus is on the different counterion-specific micelles and liquid crystals formed. These have been detected and characterized via optical microscopy, SAXS, and NMR. All Cl−PFPE surfactants form lamellar and cubic liquid crystals independently of chain length and counterion. Nonspherical micelles for the shortest PFPE chain surfactants and anomalous swelling of the lamellar phases for almost all surfactants were ascertained.

## 1. Introduction

The special properties of fluorinated surfactants have been exploited in many applications. They are of general interest for the understanding of surfactant self-assembly.[1]

The relationship between molecular structure and local curvature of the surfactant interface as a function of temperature and concentration is a key to the understanding of macroscopic phases that form, liquid crystalline phase morphology, and rheological behavior. Local curvature set by interfacial forces embodied in the packing parameter ($v/al$, where $v$ is the hydrophobic chain volume, $a$ is the polar head area, and $l$ is the hydrophobic chain length), taken together with global packing constraints set by volume fraction, allow microstructure to be predicted, including cubic and other hyperbolic geometries.[2]

There is extensive knowledge on surfactants with hydrocarbon tails. Fluorocarbon-tailed surfactant phase behavior has been much less explored. Substitution of the large, highly electronegative, fluorine atom for the smaller hydrogen atom causes significant modifications of physical and chemical properties. The increased hydrophobicity of the chain lowers surface tension and critical micelle concentrations (cmcs). The fluorocarbon chain, with a lipophilic chain volume higher than that of the hydrocarbon chain, is stiffer, and van der Waals interactions among the chains are weaker. Even a single fluorine atom in a surfactant molecule can modify packing features and phase behavior.[3] In recent investigations the effects of adding fluorinated chains to various types of ionic and nonionic surfactants have been explored by SAXS, SANS, and NMR techniques.[4,5]

Features of self-assembly of various ammonium salts of perfluoropolyether (PFPE) acids, with molecular weights (MWs) in the range of 400−900, have been reported in several papers.[6−11] Previous studies on these PFPE surfactants focused on the carboxylic salts obtained by purification and distillation of raw acidic mixtures produced via photooxidation of hexafluoropropene,[12] resulting in a perfluoroalkyl-terminated hydrophobic tail. Another process, based on the co-oxypolymerization of chlorotrifluoroethylene and hexafluoropropene,[13,14] leads to acidic mixtures with the following general structure:

$$Cl-(C_3F_6O)-(C_3F_6O)_{n-1}-CF_2COO^-X^+$$

where $X^+ = Na^+$, $K^+$, or $NH_4^+$ and $n$= 2 (n2), 3 (n3), 4 (n4).

The phase behavior in water of $Na^+$, $K^+$, and $NH_4^+$ salts of a perfluoropolyether carboxylic mixture (mostly $Cl-(C_3F_6O)$-terminated, indicated as Cl−PFPE−X, where X is the counterion) was studied recently,[15] focusing on the effects of counterion hydration and binding on packing properties. In that case, the carboxylic mixtures of interest had an average MW of about 504 corresponding to an average number of PFPE units of 2.3. At concentrations exceeding the cmc, the binding ($\beta$) of the counterion to the micelles increases in the order $\beta_{Na+} < \beta_{K+} < \beta_{NH4+}$. The extension of the micellar solution region in the binary phase diagrams increases in the order $NH_4^+ < K^+ < Na^+$, though the difference between ammonium and potassium is small. In the micellar region, the higher hydration of the sodium counterion, evidenced by a lower $\beta$, leads to the highest solubility of Cl−PFPE−Na in water. The three Cl−PFPE−X surfactants formed lamellar phases in intermediate ranges of concentration. The difference in the packing features due to counterion type showed up strongly at high surfactant concentration. Indeed, significantly different liquid crystals (LCs) were observed. A cubic phase (presumably bicontinuous) for sodium, a lamellar phase for ammonium, and a reverse hexagonal phase occurred for the potassium salt. The kind of LC phases can easily be related to an increase of the packing parameter $v/al$, as defined by Mitchell and Ninham,[16] in the sequence $Na^+ < NH_4^+ < K^+$. This trend agrees with the higher hydration number ($n_b = 6$) and with the lower binding ($\beta = 0.23$) observed for Cl−PFPE−Na. The lower hydration ($n_b = 4$) and dissociation ($\beta = 0.31$ and 0.40) observed for Cl−PFPE−K and Cl−PFPE−$NH_4$, respectively, bring about the two different arrangements, e.g., lamellar and lamellar/hexagonal phases.

This work focuses on the phase behavior of these Cl−PFPE−X ($X = Na^+$, $NH_4^+$) surfactants, obtained now with a

* To whom correspondence should be addressed. Phone: +39 070 675 4385. Fax: +39 070 675 4388. E-mail: monduzzi@unica.it.

[†] CSGI-Cagliari University.

[‡] Australia National University. Visiting Professor at Cagliari University and Florence University.

10.1021/jp049696z CCC: $27.50 
Published on Web 10/23/2004

very narrow distribution of MWs with respect to the chemical formula given above, and having different chain length (n2, n3, n4). The MWs of the carboxylate residues are 461, 627, and 793 for n2, n3, and n4, respectively. In this context, the surfactants are indicated as Na-n2, Na-n3, Na-n4 (homologues with Na counterion) and $NH_4$-n2, $NH_4$-n3, $NH_4$-n4 (homologues having $NH_4$ counterion). Some preliminary characterizations of the surface properties in water and in multicomponent systems have been reported recently.[17] In another paper the mixed micellar systems obtained by sodium or ammonium n2/n3 or n2/n3/n4 mixtures have been investigated through $^{19}F$ NMR.[18] Here, optical microscopy, NMR, and SAXS measurements were carried out.

## 2. Experimental Section

**2.1. Materials.** All the surfactant salts had purity of at least 99% with respect to the formulas above. Purity of 99.8% and 99.5% was achieved with the n2 and n3 salts, respectively. See refs 12−14 and 17 for synthesis and chemical characterization details. The surfactant/water samples were prepared, as previously reported,[7,15] using distilled water purified through a MilliQ apparatus. The surface tension of water at 25 °C was 72 mN/m. For some NMR studies, $^2H_2O$ (Carlo Erba, 99.8% enriched) was used.

To define the binary phase diagram in the liquid crystalline regions, each sample, in flame-sealed glass tubes, was homogenized through centrifugation recycling. Prior to observation, each sample was stored at 25 °C for 3 months at least. The occurrence of anisotropic phases was detected by crossed polarizers and optical microscopy.

**2.2. Methods.** The liquid crystalline phases were observed in polarized light by an optical microscope, Zeiss Universal II.

The $^1H$, $^2H$, and $^{19}F$ NMR experiments were performed by a Bruker Avance 300 (7.05 T) spectrometer at 300, 46.072, and 282.195 MHz, respectively, at 25 °C. The accuracy of temperature control was within 0.5 °C. $^2H$ NMR spectra were recorded without lock, and the error in the quadrupolar splitting measurements was around 5%. The spectra were periodically recorded to verify the attainment of equilibrium. The samples were stored at the temperature selected for each experiment. They were heated for 1 h at temperature 5 °C higher and left for 30 min in the NMR probe to ensure thermal equilibrium and alignment in the magnetic field, before recording the spectra.

Nuclei with a spin quantum number $I \geq 1$, such as $^2H$, have an electric quadrupolar moment that can interact with nonzero net electric field gradients giving multiple resonance of $2I$ peaks,[19,20] separated by the splitting:

$$\Delta\nu_q = (3/m)P_b\chi S_b \qquad (1)$$

where $m = 4$ and $m = 8$ for the lamellar and hexagonal phases, respectively, $P_b$ is the fraction of the observed nucleus in the bound state, $\chi$ is the quadrupolar coupling constant, and $S_b = 1/2(3\cos^2\vartheta_D - 1)$ is the order parameter related to the average time orientation ($\vartheta_D$) of the nucleus with respect to the surfactant chain axis. For water molecules, $P_b$ is linearly dependent on the surfactant/water ($s/w$) molar ratio and thus eq 1 can be rewritten as[20]

$$\Delta\nu_q = (3/m)n_b(s/w)\chi S_b \qquad (2)$$

where $n_b$ is the number of bound water molecules per polar head. The straight line of eq 2 would pass through the origin at low surfactant concentration.

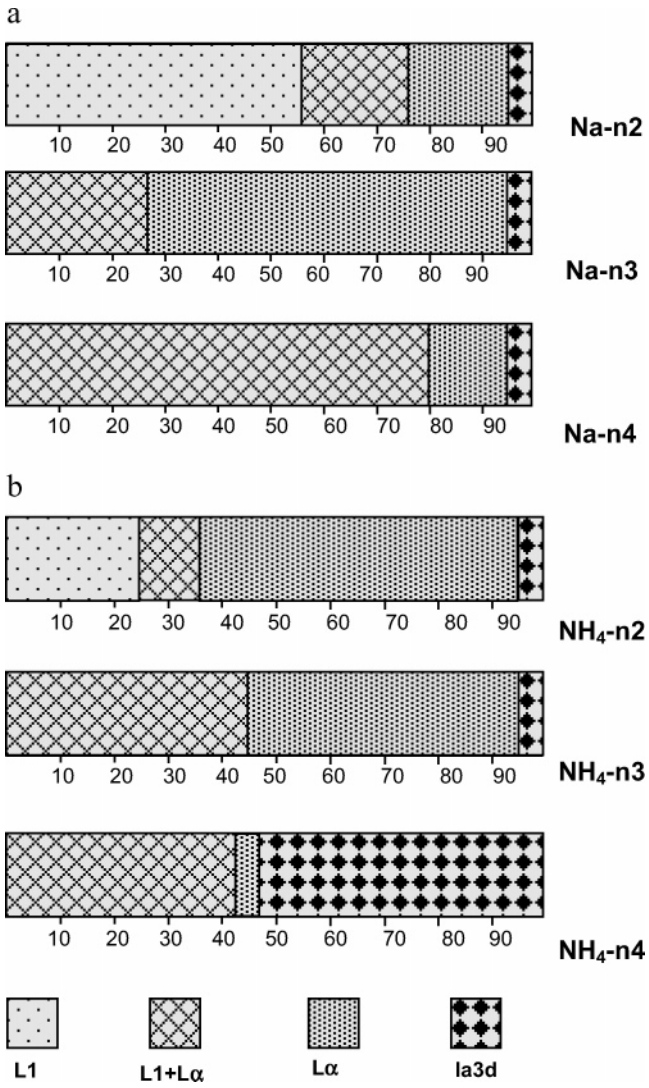


**Figure 1.** Binary phase diagrams of PFPE surfactants with different chain lengths (n2, n3, and n4) and respectively $Na^+$ counterion (a) and $NH_4^+$ counterion (b): $L_1$, micellar solution; $L_\alpha$, lamellar liquid crystal; *Ia3d*, cubic bicontinuous liquid crystal.

Diffusion measurements were performed using a DIFF30 Bruker probe equipped with a specific insert for each nucleus. The Fourier-transformed pulsed gradient spin−echo (FT-PGSE) technique was used as described by Stilbs.[21,22] The experiments were carried out by varying the gradient strength ($G$) while keeping the gradient pulse length ($\delta$) and the pulse interval ($\Delta$) constant. The decay of the echo intensity $A(G)$ with increasing $G$ values is given by

$$A(G) = A_o \exp[-D(\gamma G\delta)^2(\Delta - \delta/3)] \qquad (3)$$

where $D$ is the self-diffusion coefficient, $A_o$ is the echo intensity in the absence of any gradient, and $\gamma$ is the gyromagnetic ratio. Due to short spin−spin relaxation times of the NMR signals, surfactant self-diffusion coefficients have been determined through the stimulated echo pulse sequence to improve the signal-to-noise ratio. The self-diffusion coefficients were calculated by means of a two-parameter nonlinear fit of eq 3. The error in the measurements, as judged by repeated measurements, was estimated lower than ±5%.

SAXS data of the liquid crystals were obtained at 25 °C by means of a Kratky compact small-angle system equipped with a position sensitive detector (OED 50M from Mbraun, Graz,

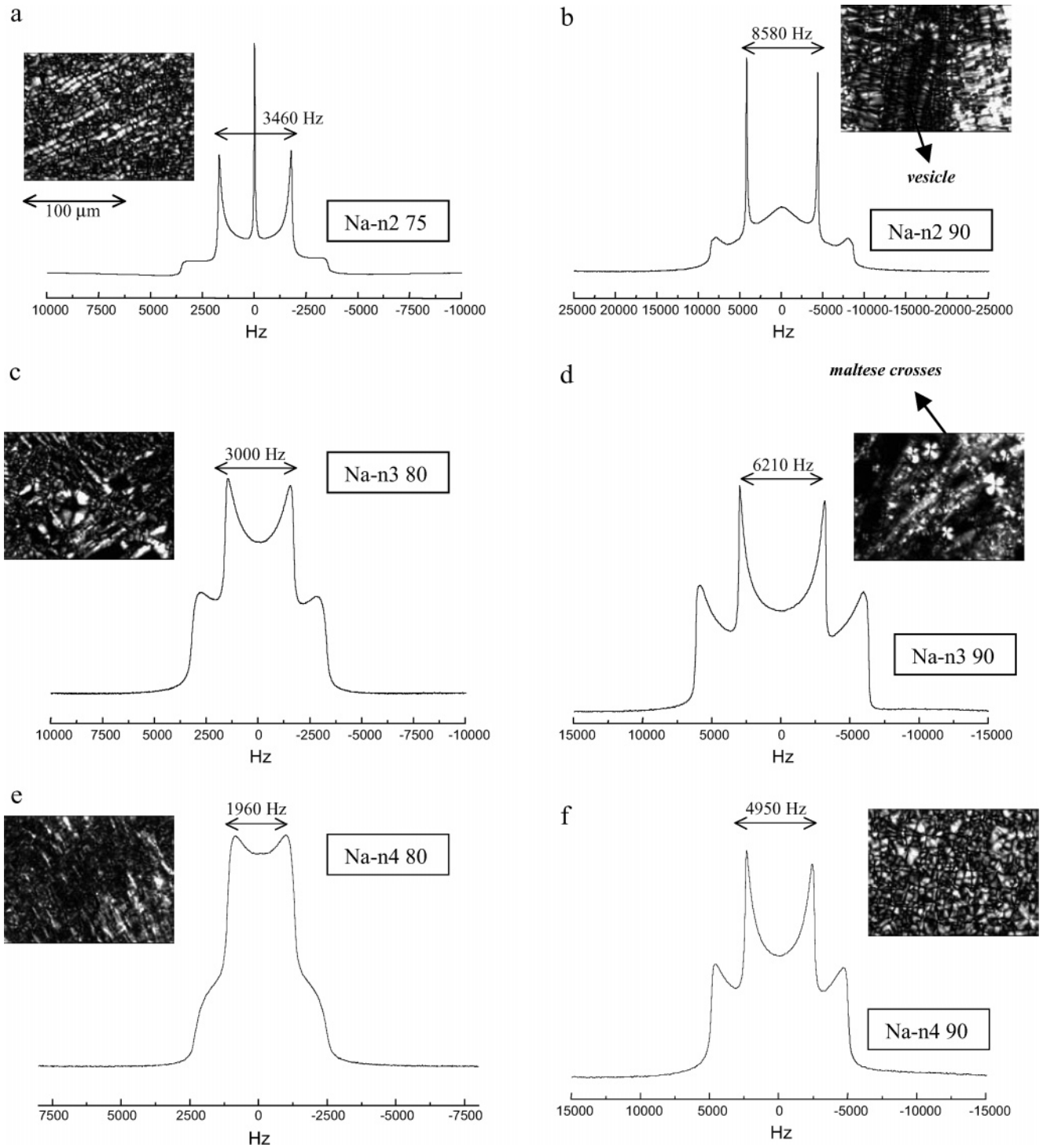


**Figure 2.** $^2$H NMR spectra showing the quadrupolar splittings for different binary Na-surfactant/$^2H_2O$ samples and relative optical micrographs in polarized light: (a) Na-n2, 75%; (b) Na-n2, 90%; (c) Na-n3, 80%; (d) Na-n3, 90%; (e) Na-n4, 80%; (f) Na-n4, 90%.

Austria) containing 1024 channels of width 51.3 mm. The Cu Kα nickel-filtered radiation of wavelength 1.542 Å was provided by a Seifert IF 300 X-ray generator operating at 50 kV and 40 mA, and the sample-to-detector distance was 27.7 cm. Temperature control within 0.1 °C was achieved by using a Peltier element.

## 3. Results and Discussion

**3.1. Phase Diagrams, Optical Microscopy, and $^2$H NMR Spectroscopy.** The binary phase diagrams were determined by visual inspection, optical microscopy, and NMR. $^2H_2O$ was used to enable $^2$H NMR measurements. The analysis of $^2$H NMR quadrupolar splittings was selected to study the concentrated phases of the surfactants (*s*). The technique gives an informative response even in the presence of multiphase samples.

The phase diagrams of Figure 1a,b are for surfactants having sodium and ammonium counterions, respectively. They are based on observations of the samples aged at 25 °C for at least 12 months. At 25 °C, the solubility limits of the surfactants in water are approximately 55 wt % for Na-n2 and 25 wt % for $NH_4$-n2. Hence, the extension of the $L_1$ micellar region decreases in the order $Na^+ \gg NH_4^+$ in agreement with the trends of

counterion hydration and binding to the micelles previously observed for the less pure surfactants. Micellar self-assembly is indeed favored by counterion dissociation.[15] This increases the electrostatic repulsion among the polar heads and promotes a positive curvature ($H > 0$) of the surfactant interface. (We are well-aware of recent developments in theories of the double layer and DLVO (Deryagin-Landau-Verwey-Overbeek) theory that show that dispersion forces combined with hydration effects dominate interactions at all but very low electrolyte concentrations. But in the strong binding case and low concentrations the conventional ion binding models capture the essence of the problem.[23]) The extension of $L_1$ phases for the homologues with higher MW is lower than 1 wt % of surfactant. Indeed the n3 and n4 surfactants, having very low solubility at 25 °C, do not present relevant monophasic micellar solution regions ($L_1$). Instead wide biphasic regions, where an isotropic solution (presumably a $L_1$ phase) and $L_\alpha$ LC coexist, are observed for n3 and n4 types. It should be recalled that cmcs around $(1-2) \times 10^{-2}$ and $(1-2) \times 10^{-3}$ M were measured for n2 and n3 PFPE surfactants, respectively, with both Na and $NH_4$ counterions at 25 °C.[18] In the case of n4 Cl−PFPE surfactants, cmc values of $(6-8) \times 10^{-6}$ M were determined only at 40 °C.[17] Indeed $^{19}F$ NMR spectra of $10^{-4}$ M solutions of n4 surfactants show at 25 °C marked broadening of the signals; solubility is very low due to Krafft temperatures higher than 25 °C. As a consequence, the regions indicated in Figure 1 as $L_1 + L_\alpha$, particularly those relative to Na-n4 and $NH_4$-n4 surfactants, may not contain real micelles. With increasing *s* concentration, all surfactants form a $L_\alpha$ LC phase, which becomes quite wide for Na-n3, $NH_4$-n2, and $NH_4$-n3. Then, with a further increase of *s* concentration, $L_\alpha$ LCs evolve toward cubic arrangements. An exceptionally wide cubic region, typically for $s \geq 48$ wt %, is observed for the $NH_4$-n4 surfactant. Provided that the occurrence of $L_\alpha$ LC was confirmed by optical microscopy and SAXS measurements (see below), the use of $^2H$ NMR allowed identification of monophasic and biphasic regions with a precision of $\pm 3-5$ wt % (this depends on the resolution of the $^2H$ NMR spectra). Some typical $^2H$ NMR spectra are reported in Figure 2 for the Cl−PFPE−Na series and Figure 3 for the Cl−PFPE−$NH_4$ series along with the corresponding optical micrographs in polarized light (except in Figure 3c where the $^2H$ NMR spectrum of an isotropic cubic phase is shown). When anisotropic LCs orient in the magnetic field, also the deuterated water molecules in the vicinity of the oriented polar−apolar interface experience anisotropic environment. This induces quadrupolar splittings $\Delta\nu_q$ which typically appear as two doublets corresponding to the perpendicular (internal doublet) and to the parallel orientation. When isotropic and anisotropic phases coexist, this can be clearly monitored in the $^2H$ NMR spectra as shown for instance in Figure 2a for Na-n2 with $s = 75$ wt %. The occurrence of $L_\alpha$ LC is clearly documented by the corresponding optical micrograph. The very broad, apparently isotropic, peak appearing at the center of the internal doublet of the Na-n2 sample ($s = 90$ wt %), shown in Figure 2b, is likely to have a different origin. It may be ascribed to the occurrence of very large vesicular domains dispersed within the lamellar packing as suggested by the corresponding optical micrograph. It may also arise from the presence of small domains of cubic phase, but no phase separation after long centrifugation occurred. Moreover, no evidence of cubic phase was observed in the SAXS spectra.

Indeed many $L_\alpha$ LC samples, particularly those at high *s* concentration, display very different optical microscopy textures and also $^2H$ NMR spectra with anomalous shapes of the doublets

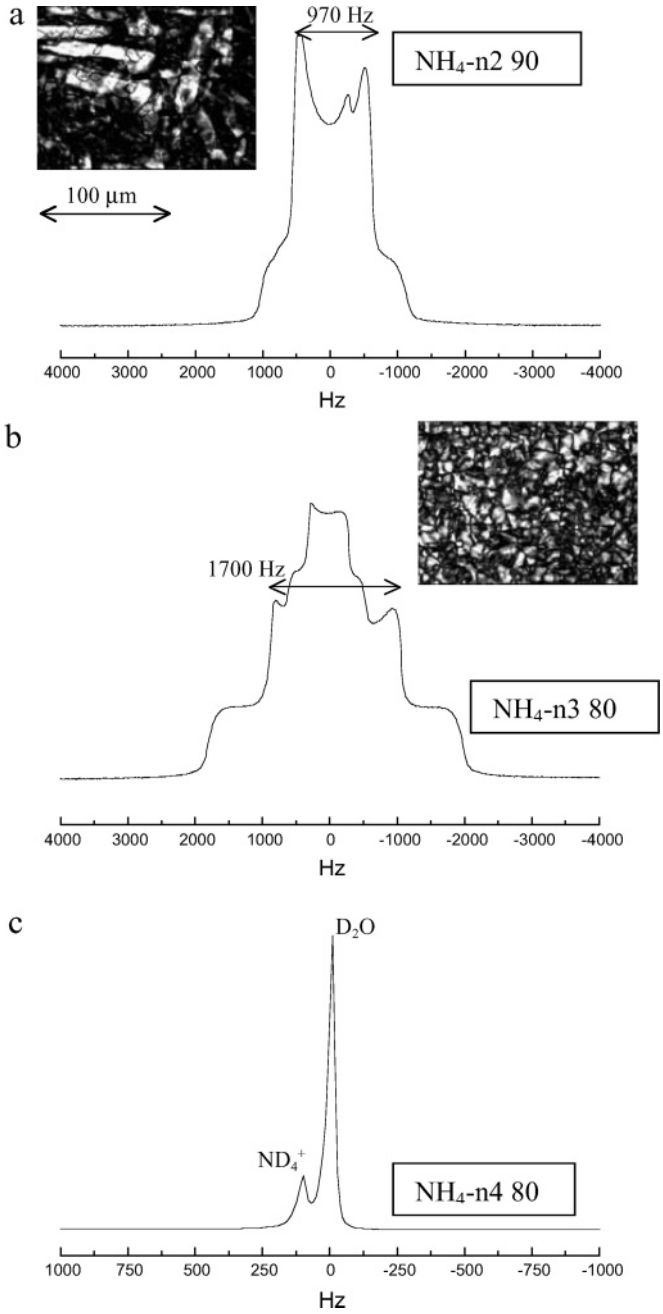


**Figure 3.** $^2H$ NMR spectra showing the quadrupolar splittings for different binary $NH_4$-surfactant/$^2H_2O$ samples and relative optical micrographs in polarized light: (a) $NH_4$-n2, 90%; (b) $NH_4$-n3, 80%; (c) $NH_4$-n4, 80%. All samples show slow exchange between $NH_4$ and $ND_4$.

(powder patterns), as reported in Figures 2 and 3. It should be noted that the interpretation of $^2H$ NMR spectra for the $NH_4$ surfactant series, particularly at high *s* concentration (see Figure 3a,b) is complicated by the occurrence of slow exchange between ammonium and water deuterons. However, the separation of the two signals is easily accomplished on the basis of the different chemical shifts (see $NH_4$-n4 in the cubic phase reported in Figure 3c), as demonstrated in previous papers.[7,15]

The attainment of equilibrium was a crucial factor for all samples in the concentrated regions of the binary phase diagrams. In any case, before recording the spectra, the samples were left in the magnetic field while the temperature was gradually decreased from 70 to 25 °C, to favor a slow alignment in the magnetic field. Nevertheless the $^2H$ NMR spectra show low resolution; that is, the samples do not easily align in the

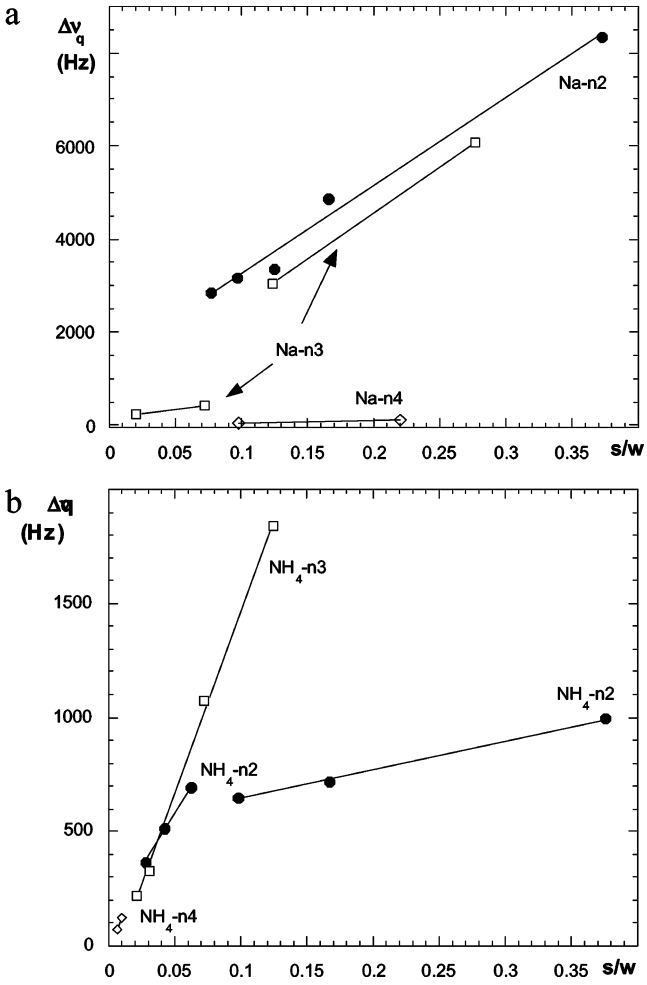


**Figure 4.** Plot of the $^2$H $\Delta\nu_q$ values vs *s*/*w* molar ratio. Different slopes indicate the existence of different types of lamellar packing. (a) Cl−PFPE−Na series: (●) Na-n2, (□) Na-n3, and (◇) Na-n4. (b) Cl−PFPE−$NH_4$ series: (●) $NH_4$-n2, (□) $NH_4$-n3, and (◇) $NH_4$-n4.

magnetic field. For several samples the 0° orientation (external doublet) could not be resolved, as shown for Na-n4 ($s = 80$ wt %) in Figure 2e and for NH4-n2 ($s = 90$ wt %) in Figure 3a, even after several cooling−heating cycles (in the range of 70−25 °C) of the samples inserted in the magnetic field.

**3.2. Anomalous Behavior.** The plot of the $^2$H $\Delta\nu_q$ values, measured in the $L_\alpha$ phases, as a function of *s*/*w* molar ratio indicated the existence of different types of lamellar packing. The results are shown in Figure 4a for the homologues with Na counterion and Figure 4b for those with $NH_4$ counterion. Straight lines crossing zero, in agreement with eq 2, would have been expected for ideal swelling. In other words, this means constant hydration of the polar groups at the bilayer interface ($n_b$) and constant product of the quadrupolar coupling constant and order parameter ($\chi S_b$). Agreement with the ideal swelling behavior is observed only for $NH_4$-n4 in the range of 20−30 wt % of the biphasic region ($L_1 + L_\alpha$) and $NH_4$-n3 in the range of 40−80% (pure $L_\alpha$ region). Acceptable agreement can be found for Na-n3 in the diluted $L_\alpha$ phase, in the range of 40−70 wt %; then, at higher *s*/*w* values a very different slope is found. It is relevant the dramatic change of slope in the quadrupolar splittings observed for $NH_4$-n2, as shown in Figure 4b. In most cases the straight lines which fit the experimental values do not pass through the expected zero value. However, what is rather surprising is the number of different slopes observed in these homologous surfactants, which have the same type of chain. The most probable explanation, at a qualitative level, follows from observation of the optical microscopy textures reported in Figures 2 and 3. Na-n2 shows a mosaic texture, typical of close-packed $L_\alpha$ bilayers, at $s = 75$ wt % (in the biphasic region) and large vesicles at $s = 90$ wt %. Na-n3 shows maltese-cross texture, typical of multilayer vesicles, at either $s = 80$ or 90 wt %. Na-n4 shows a dominant mosaic texture at $s = 90$ wt % but not at $s = 80$ wt %. For $NH_4$ surfactant series the mosaic texture is observed for $NH_4$-n3 at $s = 80$ wt % but not for $NH_4$-n2 at $s = 90$ wt %. Substantially the coexistence of close-packed and swollen $L_\alpha$ bilayers with perhaps unilamellar large vesicles and multilayer vesicles (onion-like) determine the different slopes of the $\Delta\nu_q$ trends and the deviations from ideal swelling.

The irregular swelling, visualized in terms of eq 2 and giving straight lines which do not cross through zero, may also suggest the presence of intermediate phases such as rectangular and trigonal packing as earlier characterized by Tiddy et al.[20,24,25] Indeed in recent papers on the phase behavior of the cationic fluorosurfactant 1,1,2,2-tetrahydroperfluorodecylpiridinium chloride in $^2H_2O$,[26,27] the trigonal LC phase displayed similar trends of the residual quadrupolar coupling constant (which is linearly dependent on $\Delta\nu_q$),[27] while retaining $^2$H NMR spectra with shapes very similar to those here reported in Figures 2c−e. However, this hypothesis must be ruled out since SAXS spectra (see below) always confirmed the dominant occurrence of a lamellar diffraction pattern as well as the irregular swelling.

In fact such complicated microstructural changes with change in surfactant concentration have been predicted as long ago as 1980 by Mitchell and Ninham.[16] The considerations are quite general and not model-dependent. As the surfactant parameter varies (due to changes in accessible hydration water and binding, due to interaggregate interactions) from $v/al = 1/2$ to $v/al = 1$ the theoretical prediction of what happens depends on an additional parameter, the chain flexibility or "stiffness". As $v/al$ increases, the system can transit from hexagonal phase to unilamellar vesicles which grow to polydispersed multilamellar vesicles to eventually form lamellar phase at $v/al = 1$. Alternatively it can transit first to lamellar phase, which reduces with increasing $v/al$, to smaller multilamellar vesicles, and unilamellar vesicles. With further increase in $v/al$, it returns to the lamellar phase again. Cubic phases can occur when $v/al > 0.84$.[23,28,29] While apparently counterintuitive, the predictions emerge quite naturally. They are a consequence of necessary asymmetry of curved bilayers. Inner (negative curvature) and outer (positive curvature) monolayers of surfactant molecules face very different local packing constraints that depend on chain flexibility. Indeed a variety of microstructures, with different degrees of order, and of phase transitions has been reported for fluorosurfactants.[30] Examples are the spherical micelles of lithium perfluorononanoate, the vesicles of diethylammonium perfluorooctanoate, the short rodlike micelles of ammonium perfluorooctanoate,[3,31] and also the transition from globular to long threadlike micelles of 1,1,2,2-tetrahydroperfluorodecylpiridinium chloride reported as an effect of salt addition.[26] In addition the phase diagrams of a series of perfluorononanoates[32] with different counterions showed that a lamellar packing is generally the first LC phase formed, as in the present work. Substantially flurocarbon surfactants often tend to self-assemble with more flat curvature than hydrocarbon surfactants with similar physical characteristics. Ultimately, in the case of our Cl−PFPE the terminal chlorine along with the lateral $-CF_3$ groups seem to be responsible of further hindrance and stiffness of the fluorinated chains, which induce defects in the lamellar packing and thus an anomalous swelling. This is qualitatively demon-

**TABLE 1: SAXS Data for the Lamellar ($L_\alpha$) Samples of Cl−PFPE−Na Surfactants**

| | composition (wt %) | | | | | |
|---|---|---|---|---|---|---|
| $L_\alpha$ | surfactant | water | $d$ (Å) | $h^2+k^2+l^2$ | $D$ (Å) | $l_c$ (Å) |
| Na-n2 | 70 | 30 | 27.19 | 1 | 27.19 | 9.41 |
| | | | 13.53 | 2 | 27.06 | |
| | 85 | 15 | 25.02 | 1 | 25.02 | 10.60 |
| | | | 12.51 | 2 | 25.02 | |
| Na-n3 | 20 | 80 | 176.7 | 1 | 176.7 | 15.98 |
| | | | 85.72 | 2 | 171.4 | |
| | | | 57.70 | 3 | 173.1 | |
| | 40 | 60 | 70.68 | 1 | 70.68 | 13.60 |
| | | | 34.91 | 2 | 69.82 | |
| | 70 | 30 | 47.93 | 1 | 47.93 | 16.60 |
| | 85 | 15 | 29.76 | 1 | 29.76 | 12.60 |
| | | | 14.80 | 2 | 29.60 | |
| Na-n4 | 20 | 80 | 222.3 | 1 | 222.3 | 20.28 |
| | | | 111.17 | 2 | 222.3 | |
| | | | 72.25 | 3 | 216.75 | |
| | 40 | 60 | 97.56 | 1 | 97.56 | 18.76 |
| | | | 47.93 | 2 | 95.85 | |
| | 70 | 30 | 50.51 | 1 | 50.51 | 17.45 |
| | | | 25.02 | 2 | 50.04 | |
| | 85 | 15 | 34.91 | 1 | 34.91 | 14.8 |
| | | | 17.45 | 2 | 34.91 | |

strated by the shape of the $^2$H NMR spectra and also by the different textures of optical micrographs (see Figures 2 and 3). These microstructural variety and transitions are probably enhanced in the presence of different chain lengths and/or different fluorinated groups as previously described.[15]

**3.3. Comparison with Previous Results.** It is remarkable that all Cl−PFPE surfactants here investigated form $L_\alpha$ and isotropic cubic phases independently of chain lengths and counterions. The presence of PFPE units in the chain induces a packing parameter always close to unity; hence, an average zero curvature of the polar−apolar interface is obtained. In the case of PFPE chains having a broader MW distribution, the counterion and its hydration were shown to play on the contrary a significant role.[15] The cubic phase in that case formed in the presence of Na counterion only. K counterion favored the formation of $H_2$ LC, while in the presence of $NH_4$ two different types of lamellar LCs, indicative of locally different stiffness of PFPE chains, were observed.

**3.4. Cl−PFPE−Na Series: SAXS, $^1$H, and $^{19}$F NMR Self-Diffusion.** The nonideal swelling of the lamellar phases of the Cl−PFPE−Na series is nicely confirmed by SAXS measurements performed for some samples. Data are reported in Table 1, with some diffractograms shown in Figure 5. Two-four reflections were observed for all samples. While the samples at 95 wt % surfactant show diffraction patterns typical of the *Ia*3*d* space group, all of the other samples display a dominant lamellar packing. Although no doubts concerning the attribution of a lamellar pattern of the repeating distances may arise, the plot of these distances vs Miller indexes $(h^2+k^2+l^2)^{-1/2}$ does not show the expected straight lines crossing through zero. Moreover the unit cell, that is, the bilayer thickness $D$ (see Table 1), does not show a linear decrease with increasing volume fraction of the apolar domain. This is evident from the differences between the calculated values of the chain length for each surfactant. If only the $L_\alpha$ phases at 85 wt %, for which no vesicle texture appears in the optical micrographs, are considered, the chain length ($l_c$) values of 10.6, 12.6, and 14.8 Å calculated for n2, n3, and n4 chains, respectively, appear to be reliable numbers. The addition of one perfluoropropylene oxide unit corresponds to an increase of about 2 Å of the chain length. That is reasonable.

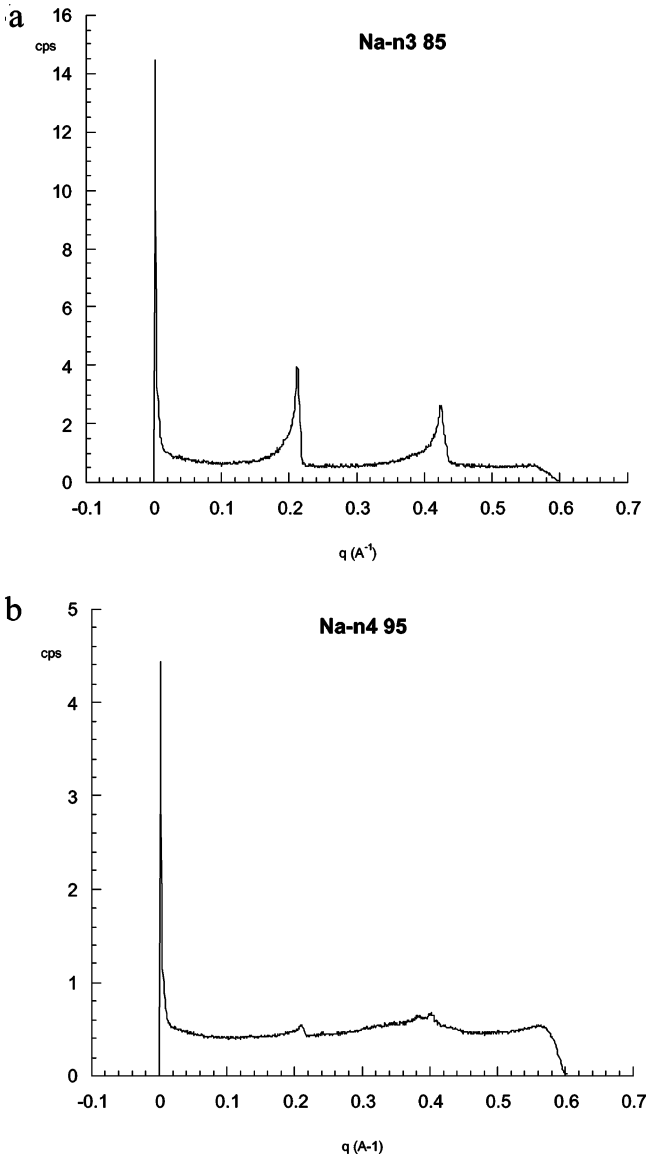


**Figure 5.** Typical SAXS patterns, cps (counts per second) vs $q$ (Å$^{-1}$), relative to (a) the lamellar phase for the sample 85 wt % Na-n3 in $H_2O$ and (b) the cubic *Ia*3*d* phase for the sample 95 wt % Na-n4 in $H_2O$.

SAXS data for the cubic phases show rather weak reflections which were assigned to the *Ia*3*d* space group, that is, a bicontinuous cubic phase constituted by a surfactant bilayer with average zero curvature ($H \approx 0$). This symmetry is often referred as cubic gyroid and described through the infinite periodical minimal surface shown in Figure 6. Differently from SAXS data for lamellar phases, the three cubic phases, for which at least three reflections were assigned, show a good agreement with Miller indexes for *Ia*3*d* cubic according to

$$d_{hkl} = (h^2+k^2+l^2)^{1/2} = 6, 8, 14, 20, 22, ... \qquad (4)$$

where $d_{hkl} = 2\pi/q$ is the repeat distance observed in the SAXS spectra. The data are shown in Table 2, and $1/d_{hkl}$ values reported vs $(h^2+k^2+l^2)^{1/2}$ are plotted in Figure 7. The straight lines nicely cross through zero, and it is worth noticing that almost the same slope is found for Na-n2, Na-n3, and Na-n4 surfactants. The length of the unit cell, that is, the long-range order, is not significantly affected by different chain lengths. That is not surprising if it is considered that the three surfactant chain lengths differ about 2−4 Å from each other.

**TABLE 2: SAXS Data for the Cubic Samples of Cl−PFPE−Na Surfactants**

| | composi tion (wt %) | | | | | | |
|---|---|---|---|---|---|---|---|
| cubic | surfactant | water | $d$ (Å) | $h^2+k^2+l^2$ | unit cell length (Å) | | space group |
| Na-n2 | 95 | 5 | 27.45 | 6 | 67.24 | | *Ia*3*d* |
| | | | 25.71 | 8 | 72.72 | av:72.6 | |
| | | | 20.79 | 14 | 77.79 | | |
| Na-n3 | 95 | 5 | 31.76 | 6 | 77.79 | | *Ia*3*d* |
| | | | 24.17 | 8 | 68.36 | av:74.9 | |
| | | | 16.06 | 24 | 78.6 | | |
| Na-n4 | 95 | 5 | 29.76 | 6 | 72.89 | | *Ia*3*d* |
| | | | 16.44 | 20 | 73.52 | av:73.3 | |
| | | | 15.71 | 22 | 73.69 | | |

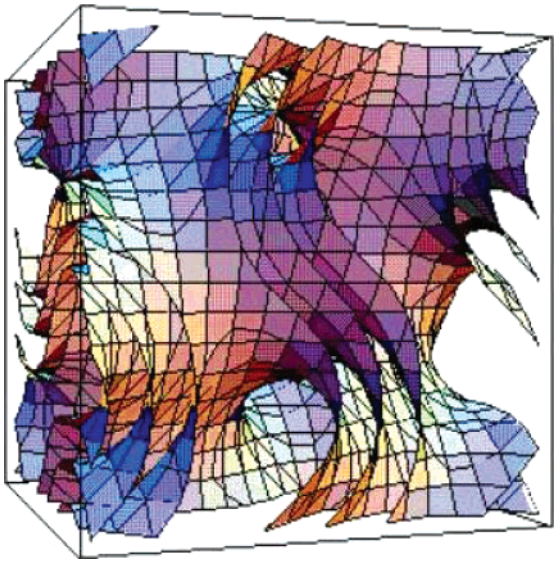

**Figure 6.** Mathematical surface of the *Ia*3*d* bicontinuous cubic phase.

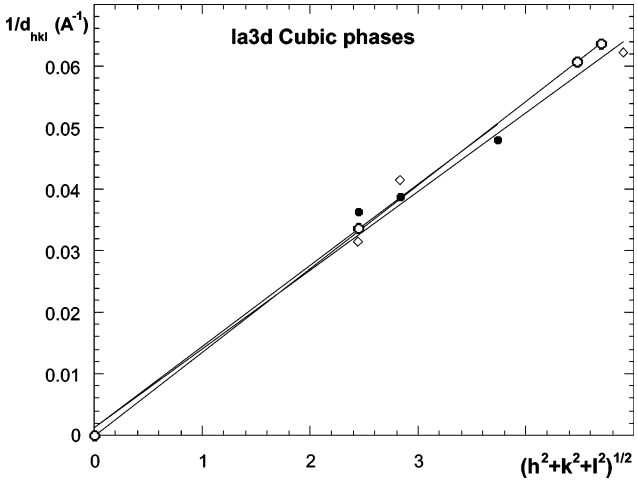


**Figure 7.** Plot of the reciprocal $d$ spacing ($1/d_{hkl}$) values reported vs $(h^2 + k^2 + l^2)^{1/2}$ for cubic *Ia*3*d* phases in the samples Na-n2 (●), Na-n3 (◇), and Na-n4 (○), all 95 wt % in water.

Further, NMR self-diffusion measurements suggest microstructural transitions within the micellar and lamellar phases. Here, only some of the results will be illustrated since they give interesting information on specific samples. First of all, we consider the micellar solution of Na-n2. Table 3 lists the measured self-diffusion coefficients of the Na-n2 $D_{surf}$ from $^{19}F$ PGSE NMR. If spherical micelles occur, the hydrodynamic micellar $R_m$ radius can be obtained, as a rough approximation, using the Stokes−Einstein relation:

$$R_m = kT/6\pi\eta D_m \tag{5}$$

where $k$ is the Boltzmann constant, $T$ is the temperature (kelvin), $\eta$ is the viscosity of water (taken as $0.89 \times 10^{-3}$ P) and $D_m \approx D_{surf}$ is the surfactant self-diffusion coefficient, mainly determined by the micelle diffusion. The calculated $R_m$ values reported in Table 3 are much greater than the chain length of about 10.6 Å obtained from SAXS data of the $L_\alpha$ phase (see Table 1). It should be remarked that eq 5 is rigorously valid only at infinite dilution, whereas at high concentration obstruction effects due to the volume fraction of the dispersed phase should be considered. Here, the dispersed phase is the surfactant volume fraction $\phi_s$. Thus, to obtain the effective micelle self-diffusion coefficient, the observed $D_{surf}$ must be corrected as follows:

$$D_{surf} = D_m^c(1 - \alpha\phi_s) \tag{6}$$

where $\alpha = 2$ if only pairwise hydrodynamic interactions are taken into account as in the case of microemulsions.[33] This is, again, a rough approximation since exchange rates of the surfactant molecules among different micelles and/or between micellar and free states are not considered. However, the $D_m^c$ self-diffusion coefficients, corrected only for the obstruction effects, and the corresponding corrected radii $R_m^c$, obtained by eq 5, are reported also in Table 3. Values still too high with respect to the chain length are calculated for a spherical micelle, particularly at $s = 40$ wt %. In addition, in the presence of spherical micelles, characterized by an equilibrium aggregation number, micellar radii should be independent of concentration. That is not the case. Indeed, because of the significant differences between the two samples, also when obstruction effects are considered, microstructural transitions may be suggested in the micellar region too. Micelles with prolate or oblate shapes, as very recently found for $NH_4$-n2,[34] and observed also for other fluorocarbon surfactants,[26] are likely to occur. According to previous papers,[35,36] the diffusion coefficient $D_m^c$ of a prolate or oblate micellar object decreases with respect to the spherical object ($D_m^{sph}$) as the axial ratio $r = a/b$ (where $b = R_o$ is the minor axis) of the prolate and oblate shape increases. Thus,

$$D_m^c = D_m^{sph}F(r) \tag{7}$$

where $F(r)$ is

$$F(r) = \{\ln[r + (r^2 - 1)^{0.5}]\}/(r^2 - 1)^{0.5} \tag{8}$$

for prolate shape and

$$F(r) = \{\arctan[(r^2 - 1)^{0.5}]\}/(r^2 - 1)^{0.5} \tag{9}$$

for oblate shape. Assuming for Na-n2 micelles a minimal radius $R_o = 10.6$ Å as obtained from SAXS measurements of the $L_\alpha$ sample at $s = 85$ wt % (see Table 1), a $D_m^{sph} \approx 2.3 \times 10^{-10}$

**TABLE 3: $^1$H and $^{19}$F Self-Diffusion Data for the Cl−PFPE−Na Series**

(a) Micellar Solutions

| surfactant/concn (wt %) | $D_{surf}$ ($10^{11}$ m$^2$/s) $^{19}$F NMR | $R_m$ (Å) | $D_m^c$ ($10^{10}$ m$^2$/s) | $R_m^c$ (Å) | $F(r) = D_m^c/D_m^{sph}$ | $r^{prol}$ | $r^{obl}$ |
|---|---|---|---|---|---|---|---|
| Na-n2/20 $\phi_s = 0.11$[a] | 9.56 | 25.6 | 1.23 | 19.9 | 0.53 | 4.0 | 2.8 |
| Na-n2/40 $\phi_s = 0.24$[a] | 2.37 | 103.3 | 45.7 | 53.7 | 0.20 | 17.0 | 7.4 |

(b) Lamellar Phases ($L_\alpha$)

| surfactant/concn (wt %) | *w*/*s* molar ratio | $D_{surf}$ ($10^{11}$ m$^2$/s) $^{19}$F NMR | $D_w$ ($10^{10}$ m$^2$/s) $^1$H NMR | water layer thickness (Å) SAXS |
|---|---|---|---|---|
| Na-n2/85−$L_\alpha$ | 4.3 | 2.73 | 2.83 | 3.8 |
| Na-n3/85−$L_\alpha$ | 5.7 | 1.74 | 4.76 | 4.5 |
| Na-n4/85−$L_\alpha$ | 7.2 | 1.27 | 5.25 | 5.3 |

(c) Bicontinuous *Ia*3*d* Cubic Phases ($C_G$)

| surfactant/concn (wt %) | *w*/*s* molar ratio | $D_{surf}$ ($10^{12}$ m$^2$/s) $^{19}$F NMR | $D_w$ ($10^{11}$ m$^2$/s) $^1$H NMR | unit cell length (Å) SAXS |
|---|---|---|---|---|
| Na-n2/95−$C_G$ | 1.3 | 1.96 | 3.24 | 72.6 |
| Na-n3/95−$C_G$ | 1.7 | 3.04 | 6.77 | 74.9 |
| Na-n4/95−$C_G$ | 2.1 | 5.12 | 9.64 | 73.3 |

[a] $\phi_s$ was calculated assuming a density of 1.8 g/mL as found for many PFPE surfactants.[15,34]

m$^2$/s is calculated for a micelle of spherical shape. In Table 3 the ratios $F(r) = D_m^c/D_m^{sph}$ and the corresponding axial ratios ($r = a/b$, where $b = R_o = 10.6$ Å) $r^{prol}$ and $r^{obl}$ calculated through eqs 8 and 9 are reported. The axial ratios of both prolate and oblate shapes are quite high, and they increase remarkably with increasing *s* concentration from 20 wt % (about 0.4 M solution) to 40 wt % (about 0.8 M solution). Indeed these data agree with the modeling of SANS data[34] for the aggregates formed by $NH_4$-n2 surfactant in the $L_1$ phase. In that work, the micelles, at 28 °C, were suggested to be sharply prolate ellipsoids, with axial ratio around 2.4, already at 0.2 M concentration and to be of spherical shape below 0.1 M concentration only.

In the case of lamellar phases which occur at 85 wt % s concentration in the Cl−PFPE−Na series, it is worth noticing the nice correlation between the *w*/*s* molar ratio and the water layer thickness calculated from SAXS along with the water self-diffusion coefficients from $^1$H PGSE NMR experiments. With increasing *w*/*s*, the water layer increases, and paralleling this, the $D_w$ values increase, while the coefficients $D_{surf}$ , obtained from $^{19}$F PGSE NMR experiments, decrease slightly due to the chain-length effect. $D_w$ does not reach the values of $2D^\circ_w/3 = 1.5 \times 10^{-9}$ m$^2$/s expected for free diffusion in a plane. This is due to the reduced amount of water. Indeed only for Na-n4, the *w*/*s* ratio corresponds to the full hydration of sodium counterions.

Interesting self-diffusion data are obtained also for the cubic phases formed at 95 wt % surfactants. With increasing *w*/*s* values $D_w$ coefficients increase. Moreover, with increasing chain length and consequently *w*/*s*, also the coefficients $D_{surf}$ increase. Both $D_w$ and $D_{surf}$ self-diffusion coefficients are almost 1 order of magnitude lower than those observed in the lamellar phase. Here, the amount of water is always below hydration needs, but the decrease may be mainly due to the significant increase of macroscopic viscosity of the cubic LC phase. Substantially $D_w$ and $D_{surf}$ self-diffusion coefficients show a parallel trend with increasing chain length. This represents a beautiful confirmation of the bicontinuity condition of these cubic phases, as already suggested by the occurrence of *Ia*3*d* symmetry from SAXS data.

Due to the limited production of these particularly pure Cl−PFPE surfactants, it was not possible to perform similar investigations on the series containing $NH_4$ counterion.

## 4. Conclusions

In this paper it has been shown that PFPE-based surfactants present a variety of microstructures and transitions within the same macroscopic monophasic region. It was shown that only $L_\alpha$ and bicontinuous cubic (*Ia*3*d* space group) LCs form independently of chain length and counterion, and differently from previous investigations where the Cl−PFPE−X surfactants with less defined formula tails were used. The occurrence of nonspherical micelles and defective lamellar phases has been suggested in agreement with other fluorosurfactants phase behavior. The reasons arise from the chemical nature of the fluorinated chains, particularly from the varying chain stiffness with chain length caused by the presence of the perfluoropropylene oxide units. These confer apparently peculiar, complex phase properties.

**Acknowledgment.** Thanks are due to Solvay Solexis−R&D Center Physical Chemistry of Interphases for fluorinated compounds and Consorzio Sistemi a Grande Interfase (CSGI, Florence) for financial support. Alba Chittofrati (Solvay Solexis) is thanked for useful discussions. Piero Baglioni (Florence University) is gratefully acknowledged for making available the SAXS spectrometer facility. B. W.N. thanks MIUR (Italy) for funding his Visiting Professor position at Cagliari and Florence Universities.

## References and Notes

(1) Kissa, E. *Fluorinated Surfactants. Synthesis. Properties. Applications*; Dekker: New York, 1994; Vol. 50.

(2) Hyde, S.; Andersson, S.; Larsson, K.; Blum, Z.; Landh, T.; Lidin, S.; Ninham, B. W. *The Language of Shape*; Elsevier: Amsterdam, 1997.

(3) Hoffmann, H.; Wurtz, J. *J. Mol. Liq.* **1997**, *72*, 191, and references therein

(4) Ropers, M. H.; Stebé, M.-J.; Schmitt, V. *J. Phys. Chem. B* **1999**, *103*, 3468.

(5) Kadi, M.; Dvinskikh, S. V.; Furo, I.; Almgren, M. *Langmuir* **2002**, *18*, 5015.

(6) Monduzzi, M.; Chittofrati, A.; Visca, M. *Langmuir* **1992**, *8*, 1278.

(7) Monduzzi, M.; Chittofrati, A.; Boselli, V. *J. Phys. Chem.* **1994**, *98*, 7591.
(8) Kallay, N.; Tomasić, V.; Zalac, S.; Chittofrati, A. *Colloid Polym. Sci.* **1994**, *272*, 1576.
(9) Tomasić, V.; Chittofrati, A.; Kallay, N. *Colloids Surf. A* **1995**, *104*, 95.
(10) Monduzzi, M.; Knackstedt, M. A.; Ninham, B. W. *J. Phys. Chem.* **1995**, *99*, 17772.
(11) Caboi, F.; Chittofrati, A.; Monduzzi, M.; Moriconi, C. *Langmuir* **1996**, *12*, 6022.
(12) Sianesi, D.; Marchionni, G.; DePasquale, R. J. PFPE Synthesis. In *Organofluorine Chemistry: Principles and Commercial Applications*; Banks, E., Smart, B. E., Tatlow, J. C., Eds.; Plenum: New York, 1994; Ch. 20.
(13) Marchionni, G.; Guarda, P. A.; De Patto, U. 11th European Symposium on Fluorine Chemistry, Bled, Slovenia, 1995.
(14) Lazzari, P.; Chittofrati, A.; Maccone, P.; Gambi, C. M. C.; Caboi, F.; Monduzzi, M. Communication at GICI-1997, Societá Chimica Italiana, Gargnano, Italy, 1997.
(15) Caboi, F.; Chittofrati, A.; Lazzari, P.; Monduzzi, M. *Colloids Surf. A* **1999**, *160*, 47.
(16) Mitchell, J. D.; Ninham, B. W. *J. Chem. Soc., Faraday Trans. 2* **1981**, *77*, 601.
(17) Chittofrati, A.; Pieri, R.; D'Aprile, F.; Lenti, D.; Maccone, P.; Visca, M. *Prog. Colloid Polym. Sci.* **2004**, *25*.
(18) Mele, S.; Murgia, S.; Monduzzi, M. *J. Fluorine Chem.* **2004**, *125*, 261.
(19) Tiddy, G. J. T. *J. Chem. Soc., Faraday Trans. 1* **1972**, *68*, 608.
(20) Tiddy, G. J. T. In *Modern Trends of Colloids Science in Chemistry and Biology*; Eicke, H. F., Ed.; Birkhauser Verlag: Basel, Switzerland, 1985; p 158.
(21) Stejskal, E. O.; Tanner, J. E. *J. Chem. Phys.* **1965**, *42*, 288.
(22) Stilbs, P. *Prog. Nucl. Magn. Reson. Spectrosc.* **1987**, *19*, 1.
(23) Mitchell, J. D.; Ninham, B. W.; Evans, D. F. *J. Phys. Chem.* **1984**, *88*, 6344.
(24) Hall, C.; Tiddy, G. J. T. In *Surfactants in Solutions*; Mittal, K. L., Ed.; Plenum: New York, 1989; Vol. 8; p 9.
(25) Kekicheff, P.; Tiddy, G. J. T. *J. Phys. Chem.* **1989**, *93*, 2520.
(26) Wang, K.; Karlsson, G.; Almgren, M.; Asakawa, T. *J. Phys. Chem. B* **1999**, *103*, 9237.
(27) Wang, K.; Oradd, G.; Almgren, M.; Asakawa, T.; Bergenståhl, B. *Langmuir* **2000**, *16*, 1042.
(28) Lisiecki, I.; Andrè, P.; Filankembo, A.; Petit, C.; Tanori, J.; Gulik-Krzywicki, T.; Ninham, B. W.; Pileni, M. P. *J. Phys. Chem. B* **1999**, *88*, 9168.
(29) Lisiecki, I.; Andrè, P.; Filankembo, A.; Petit, C.; Tanori, J.; Gulik-Krzywicki, T.; Ninham, B. W.; Pileni, M. P. *J. Phys. Chem. B* **1999**, *88*, 9176.
(30) Monduzzi, M. *Curr. Opin. Colloid Interface Sci.* **1998**, *3*, 467.
(31) Burkitt, S. J.; Ottewill, R. H.; Hayter, J. B.; Ingram, B. T. *Colloid Polym. Sci.* **1987**, *265*, 619.
(32) Fontell, K.; Lindman, B. *J. Phys. Chem.* **1983**, *87*, 3289.
(33) Caboi, F.; Capuzzi, G.; Baglioni, P.; Monduzzi, M. *J. Phys. Chem. B* **1997**, *101*, 10205.
(34) Gambi, C.; Giordano, R.; Chittofrati, A.; Pieri, R.; Baglioni, P.; Texeira, J. *J. Phys. Chem. A* **2003**, *107*, 11558.
(35) Balinov, B.; Olsson, U.; Soderman, O. *J. Phys. Chem.* **1991**, *95*, 5931.
(36) Pitzalis, P.; Angelico, R.; Soderman, O.; Monduzzi, M. *Langmuir* **2000**, *16*, 442.